ELSEVIER

Journal of Alloys and Compounds 223 (1995) 32–38

Journal of ALLOYS AND COMPOUNDS

Zr–Ti–V–Ni alloys with dendrite-free structure

D.-Y. Yan, G. Sandrock, S. Suda

Department of Chemical Engineering, Kogakuin University, 2665-1, Nakano-machi, Hachioji-shi, Tokyo 192, Japan

Received 3 June 1994; in final form 18 August 1994

Abstract

Zr–Ti–V–Ni alloys with dendrite-free structure were investigated by photomicrographs, scanning electron microscopy, electron spectroscopy for chemical analysis, electron probe microanalysis and ICPS in order to develop new cathodic hydrogen storage alloys. It has been found that the activation and kinetics of AB_2 alloys with dendrite-free structure are improved significantly. The relationship between electrochemical characteristics and dendrite-free structure is discussed.

Keywords: Dendrite-free structure; Cathodic hydrogen storage; Electrochemical characteristics

1. Introduction

Previous work has shown that among the Zr–Ti–V–Ni system alloys $Zr_{0.5}Ti_{0.5}V_{0.75}Ni_{1.25}$ displays high capacity (370 mA h g^{-1}), long cycle life and satisfactory charge retention, but poor kinetic characteristics and difficult activation [1,2]. These two problems are the main drawback of most AB_2 cathodic hydrogen storage alloys from the viewpoint of electrochemical applications. We believe that it is important to improve the kinetic characteristics and initial activation properties of AB_2 alloys to meet the requirements of commercial batteries, especially for electric vehicles.

With regard to $Zr_{0.5}Ti_{0.5}V_{0.75}Ni_{12.5}$, many efforts have been made to improve its electrochemical properties. Surface coating of alloy powders with copper by chemical plating was found to improve the high rate capability [3]. The addition of small amounts of Fe, Cr and other metallic elements, however, can only improve the corrosion resistance and the durability for charge–discharge (C–D) cycling [1,4].

Structural analysis shows that $Zr_{0.5}Ti_{0.5}V_{0.75}Ni_{1.25}$ has two structures: dendritic (about 80%) and dendrite free (about 20%) [2]. The dendritic structure exists in the V-rich phase which exhibits higher hydrogen capacity. Stronger V(Zr,Ti)–H bonding has been considered as the source of the poor kinetic property. Another possible reason considered is the transportation of hydrogen from the V-rich phase to other phases. Ni can decrease the bonding strength of V(Zr,Ti)–H, besides its catalysis of the electrochemical reaction and protection of the alloy from alkaline corrosion. It is therefore reasonable to increase the Ni content to reduce the dendritic structure. Reduction of the relative amount of V-rich phase is thought to improve the kinetic and activation properties of the alloy.

The aim of this work is to investigate the relationship between dendrite-free structure and electrochemical characteristics for $Zr_{0.5}Ti_{0.5}V_{0.75}Ni_x$ alloys (denoted W_x hereinafter).

2. Experimental details

The W_x ($x = 1.25$, 1.375, 1.5, 1.625, 1.75) alloy samples were prepared by arc melting in an argon atmosphere on a water-cooled copper hearth. The raw materials were sponge Ti and Zr, crystal V and pellet Ni carbonyl. Each 25 g specimen was melted four times, being turned over each time to ensure homogeneity. The melts were cooled down as a button in the copper container. The alloys were then crushed mechanically to obtain powders of a size smaller than 26 μm. The alloy composition was determined by ICPS analysis.

Photomicrographs were employed for structure observation on an Olympus model PMG3 metallurgical microscope. The test pieces were made by mounting, polishing and etching ($95H_2O$, $4.5HNO_3$, 0.5HF). The profile section structure and element analyses were carried out by scanning electron microscopy (SEM) and electron probe microanalysis (EPMA 8705, Shimazu). The effect of annealing treatment on the $W_{1.25}$ and

Elsevier Science S.A.
SSDI 0925-8388(94)01409-4

$W_{1.5}$ alloy microstructures was investigated. The alloy samples were heated at 1000 °C for 5 h and cooled naturally to room temperature in a tube furnace under an Ar atmosphere. Composition analysis was carried out by ICPS (IMSICP-1T, Jeol). X-Ray diffraction (XRD) was performed on a Rigaku RINT-1200 diffractometer using Cu Kα radiation. Surface analyses were carried out by means of X-ray photoemission spectroscopy (XPS) (ESCA-850M, Shimazu). The XPS sample was prepared after 15 C–D cycles. The electrode was made of $W_{1.5}$ alloy powder (1 g, less than 26 μm; polytetrafluoroethylene (PTFE) and Ni_{255} were not used). It was charged at 25 mA g^{-1} for 15 h, held for 10 min, discharged at 50 mA g^{-1} to 0.9 V in 6 N KOH solution, washed with purified water until pH 7 and then dried. The base pressure in the spectrometer was 10^{-7} Pa and Mg Kα ($h\nu$=1253.6 eV) radiation was used at 10 kV and 30 mA. To measure depth profiles, Ar^+ ion bombardment (4×10^{-4} Pa) at 2 kV and 25 mA was used.

Table 1
Discharge conditions for cycles 1–35

Cycles	1–10	11–15	16–20	20–25	25–30	31–32	33–35
Rate (mA g^{-1})	200	400	600	400	200	50	100

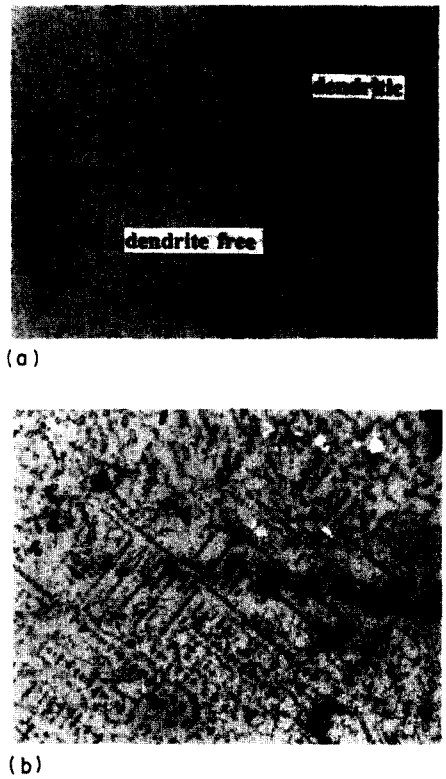

Fig. 1. Photomicrographs of $Zr_{0.5}Ti_{0.5}V_{0.75}Ni_{1.25}$ alloy with dendritic and dendrite-free structure: (a) dendritic and dendrite-free structure (magnification, ×100); (b) dendritic structure (magnification, ×400).

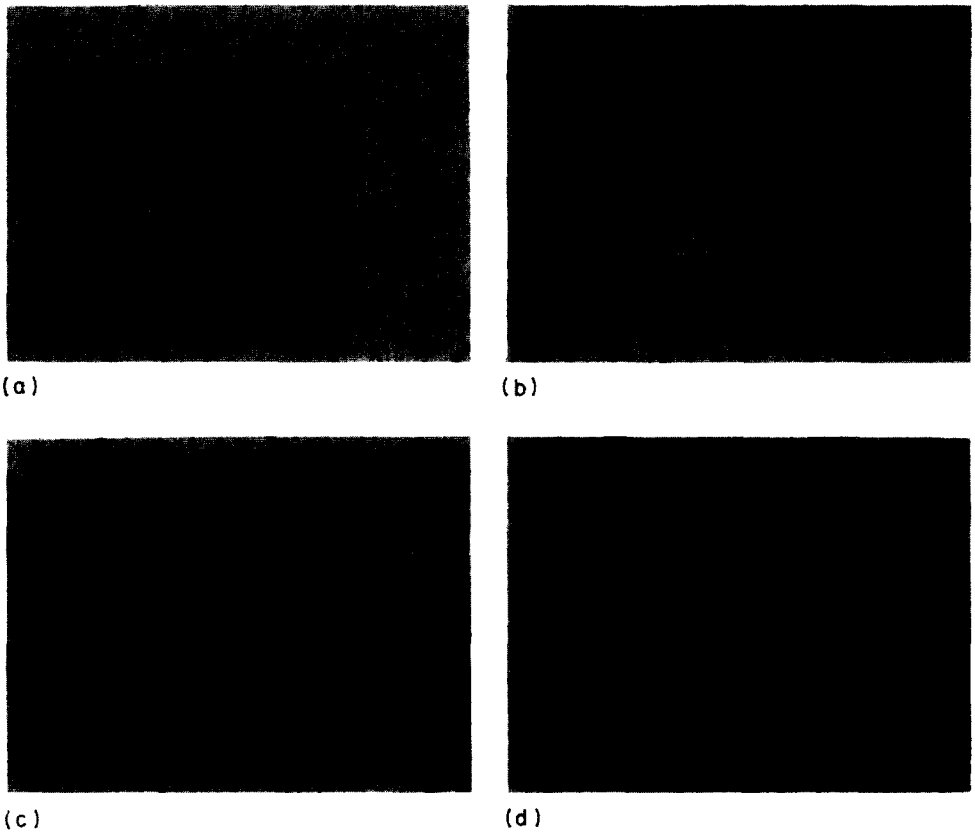

Fig. 2. Photomicrographs of $Zr_{0.5}Ti_{0.5}V_{0.75}Ni_x$ alloys with dendrite-free structure: (a) x=1.375; (b) x=1.5; (c) x=1.625; (d) x=1.75 (magnification, ×400).

An amount of alloy (0.25 g) was mixed with Ni_{255} powder (0.75 g) and PTFE (0.05 g). The mixture was sandwiched by nickel mesh and cold pressed to 4×10^8 Pa to obtain a pellet 13 mm in diameter to use as an electrode. The pellet was welded on nickel line.

The prepared electrodes were placed in the central compartment of a Pyrex cell with 6 N KOH electrolyte and an $Ni(OH)_2/NiOOH$ counterelectrode. The electrodes were charged at 200 mA g^{-1} for 2 h, held for 10 min and discharged to −0.55 V vs. Hg/HgO at 20 °C. The discharge conditions for cycles 1–35 are listed in Table 1. After the 36th cycle the discharge rate was repeated as for cycles 6–25, except that cycles 101–105 were the same as cycles 31–35.

3. Results and discussion

3.1. Alloy structure

The $W_{1.25}$ alloy has a solidification instability that leads to an inhomogeneity in its microstructure. There are some regions with dendrites and some that are dendrite free (see Figs. 1(a) and 1(b)). EPMA analysis indicates that the dendritic regions of the $W_{1.25}$ alloy consist of three or four phases: a dendritic phase very rich in V; one or two AB_2 phases containing all elements, but low V; ZrO_2. The dendrite-free regions of the $W_{1.25}$ alloy consist of: one or two AB_2 phases containing all elements, with substantial V; trace of free Ti or TiNi; ZrO_2.

Fig. 2 shows photomicrographs of the other W_x alloys. Upon increasing the Ni content above 1.375, the dendritic regions disappear. The alloys with Ni content above 1.375 are very similar to the dendrite-free regions of the $W_{1.25}$ alloy. The W_x ($x>1.375$) alloys with dendrite-free structure are seen to display excellent homogeneity and are distinctly different from $W_{1.25}$.

Exact EPMA examination shows that in the alloys with dendrite-free structure there are two major AB_2 phases: V, Zr rich; Ti, Ni rich (see Fig. 3). During solidification, alloy segregation causes very slight inhomogeneity, but the disorder is very indistinct. A $Zr_{0.495}Ti_{0.505}V_{0.771}Ni_{1.546}$ alloy ingot of 2 kg mass exhibited the same excellent homogeneity. The alloy composition was obtained by ICPS analysis. The surface and central part of the ingot were chosen to take photomicrographs (see Fig. 4). Most of the surface and the entire centre were found to be dendrite free.

X-Ray diffraction analysis indicates that $W_{1.25}$ is mainly an AB_2 C_{14} phase [2]. Figs. 5 shows that the XRD peaks are rather broad and contain some multiple subpeaks. Comparing W_x ($x>1.25$) with $W_{1.25}$, the rel-

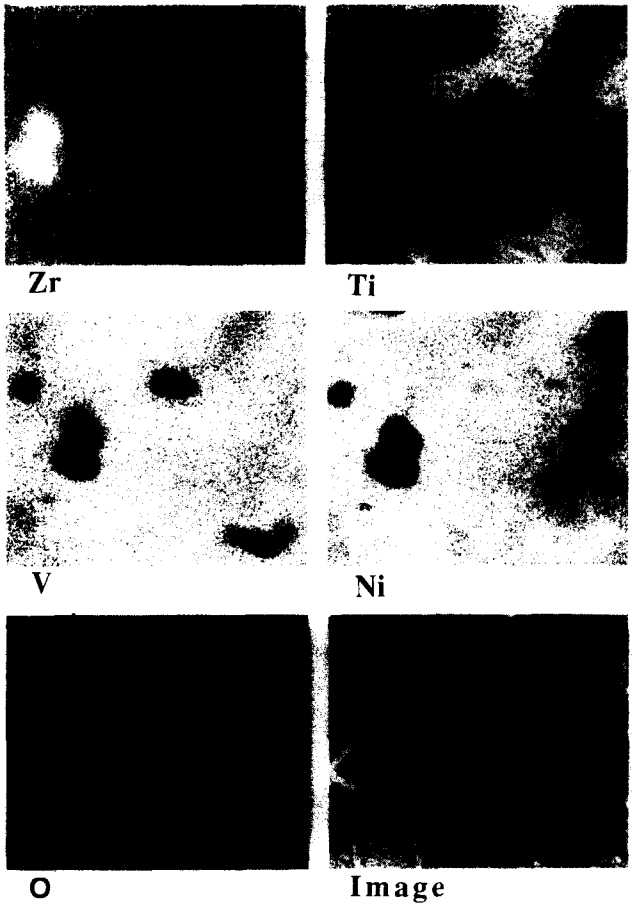

Fig. 3. EPMA surface analysis of $Zr_{0.5}Ti_{0.5}V_{0.75}Ni_{1.5}$ alloy.

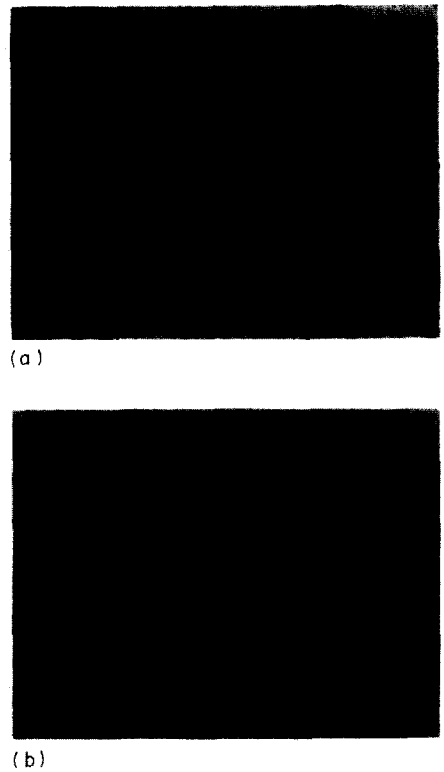

Fig. 4. Photomicrographs of $Zr_{0.495}Ti_{0.505}V_{0.771}Ni_{1.546}$ alloy ingot of 2 kg mass: (a) surface; (b) centre (magnification, ×400).

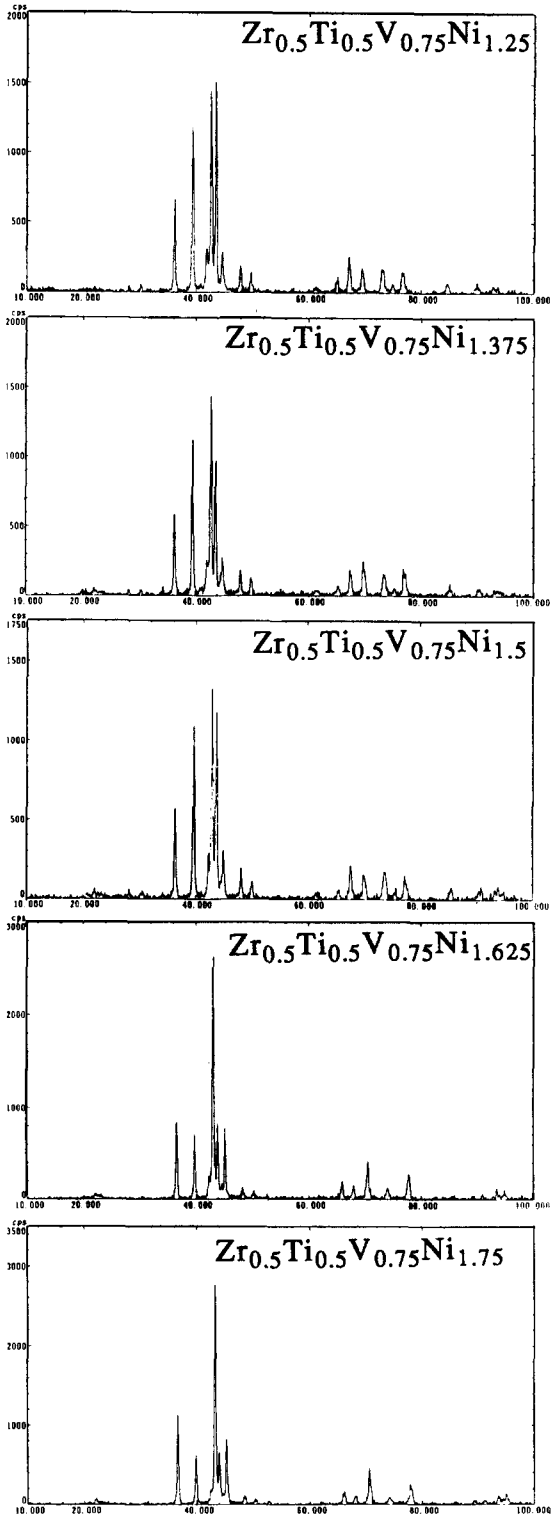

Fig. 5. X-Ray diffraction profiles of $Zr_{0.5}Ti_{0.5}V_{0.75}Ni_x$ alloys.

ative strength of diffraction peaks changes to some extent, while the diffraction peaks of W_x ($x > 1.25$) move to higher diffraction angle, since Ni is increased. No extra peaks were found in the profiles. The lattice constants are summarized in Table 2. The lattice constants and volume decreased with increasing Ni content.

Table 2
Lattice parameters of W_x alloys

Alloy	a (Å)	c (Å)	V (Å^3)
$W_{1.25}$	4.966	8.114	519.973
$W_{1.375}$	4.946	8.074	513.122
$W_{1.5}$	4.932	8.064	509.568
$W_{1.625}$	4.912	7.967	499.530
$W_{1.75}$	4.912	7.926	496.974

The previously mentioned structure analyses indicate that W_x ($x = 1.25$–1.75) is multiphase; the homogeneity is improved significantly with increased Ni content. $W_{1.25}$ is an inhomogeneous phase with dendritic structure; W_x ($x > 1.25$) alloys are homogeneous phase, hence dendrite free.

The surface structure of W_x ($x > 1.25$) was investigated by ESCA using model alloy $W_{1.5}$ cycled electrochemically. ESCA analysis shows that Zr, Ti and V form oxides on the alloy surface in alkaline solutions during C–D cycling (see Fig. 6). The Zr 3d, Ti 2p, V $2p_{3/2}$ and Ni $2p_{3/2}$ core levels were determined for $Zr_{0.5}Ti_{0.5}V_{0.75}Ni_{1.5}$, along with the spectra obtained after various sputtering periods. The test sample was charged and discharged for 15 cycles in 6 N KOH solution at lower rate (50 mA g^{-1}) at 20 °C (see Fig. 7). The chemical states were examined by determining the binding energy (E_b). The top layer of the alloy surface consists of oxides and hydroxides of the four metallic elements. There is no Ni^0 in the top layer. The sublayer consists of TiO_2 ($E_b = 459.1$ eV), ZrO_2 ($E_b = 182.4$ eV), vanadium oxides ($E_b = 522.0$ eV) and Ni^0 ($E_b = 852.7$ eV). The analysis specifically shows that the surface structure consists of Ti, Zr and V in the oxidized state with underlying metallic Ni.

The effect of thermal treatment on the $W_{1.25}$ and $W_{1.5}$ alloy microstructures was investigated. The alloy samples were heated at 1000 °C for 5 h and cooled naturally to room temperature. Fig. 8 shows photomicrographs of the thermally treated $W_{1.25}$ and $W_{1.5}$ alloys. After the thermal treatment $W_{1.25}$ continues to exhibit two structures, dendritic and dendrite free, but the boundary line between the two areas becomes rather indistinct. The thermally treated $W_{1.5}$ alloy retains its dendrite-free structure, including the ingot surface. Both treated alloys show better homogeneity than the untreated alloys.

3.2. Electrochemical characteristics

Figs. 9(a)–9(c) show discharge capacity vs. cycle curves at discharge rates of 200, 400 and 600 mA g^{-1} respectively. All W_x ($x > 1.25$) alloy electrodes exhibit higher discharge capacity and easier activation than $W_{1.25}$. The higher homogeneity of the alloys with den-

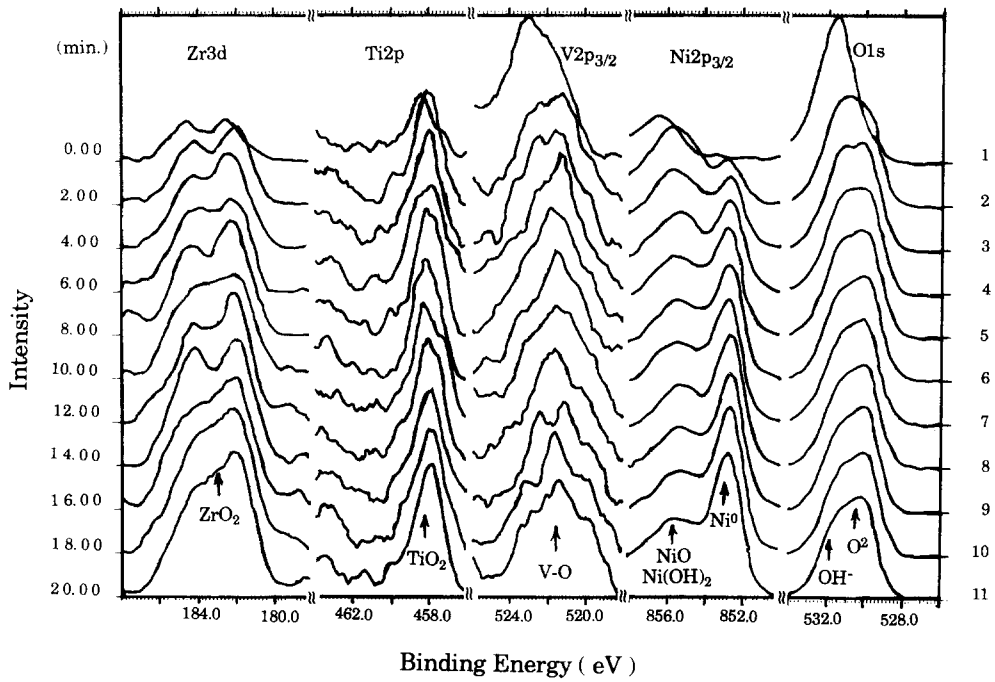

Fig. 6. Zr 3d, Ti 2p, V $2p_{3/2}$ and Ni $2p_{3/2}$ core level spectra of $Zr_{0.5}Ti_{0.5}V_{0.75}Ni_{1.5}$ alloy after 15 C–D cycles in 6 N KOH solution at 20 °C.

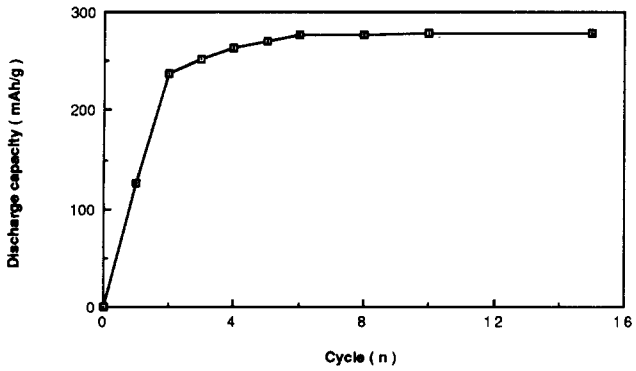

Fig. 7. Discharge capacity vs. cycle curve for $Zr_{0.5}Ti_{0.5}V_{0.75}Ni_{1.5}$ electrode made of 100% alloy (less than 26 μm; charged at 25 mA g^{-1} for 15 h, held for 10 min, discharged at 50 mA g^{-1} to 0.9 V at 20 °C).

drite-free structure accounts for the better electrochemical properties. Fig. 10 shows curves of the hydrogen storage capacity of the alloys vs. Ni content x at 50 mA g^{-1} for cycles 31 and 111. An increase in Ni content decreases the hydrogen capacity, so the Ni content should be carefully controlled. $W_{1.625}$ and $W_{1.75}$ exhibit higher discharge capacity at higher rates and also better durability, although their hydrogen capacity is lower than that of $W_{1.25}$. When the alloy electrodes had achieved their maximum discharge capacity C_{max} at 200 mA g^{-1}, the discharge capacity vs. discharge rate curves were measured (see Fig. 11). The kinetics of the alloy have been improved. C_{max} at various discharge rates and the cycle life of the W_x alloys are given in Table 3. C_{300} is the discharge capacity after 300 C–D cycles.

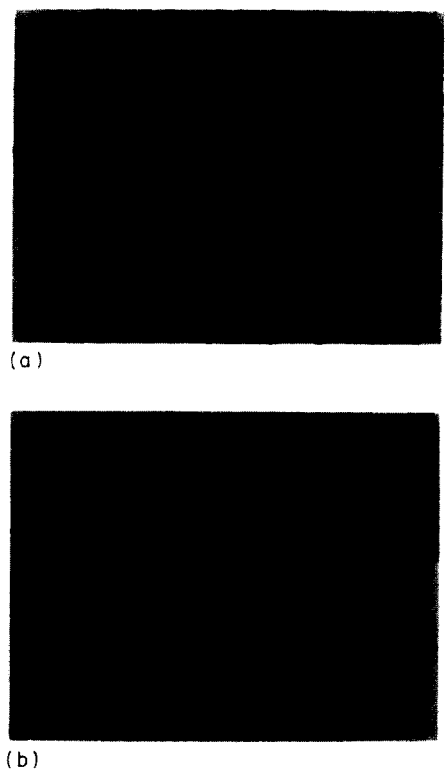

Fig. 8. Photomicrographs of thermally treated $W_{1.25}$ and $W_{1.5}$ alloys: (a) dendritic structure of treated $W_{1.25}$; (b) dendrite-free structure of treated $W_{1.5}$ (magnification, ×400).

A good correlation is obtained when r is plotted against the lattice constant c as shown in Fig. 12, while r plotted against the lattice constant a shows a similar correlation. Here r is the ratio of the discharge capacity

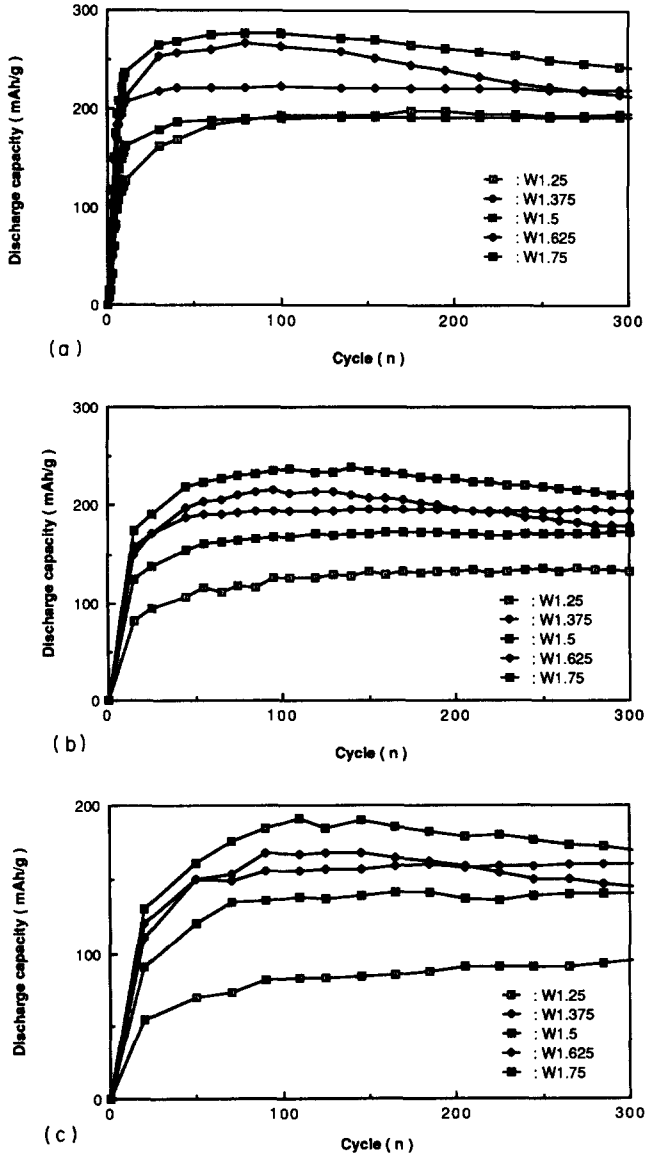

Fig. 9. Comparison of discharge capacity vs. cycle curves for $Zr_{0.5}Ti_{0.5}V_{0.75}Ni_x$ alloys at various discharge rates (charged at 200 mA g^{-1} for 2 h, held for 10 min, discharged to 0.55 V vs. Hg/HgO at 20 °C): (a) 200 mA g^{-1}; (b) 400 mA g^{-1}; (c) 600 mA g^{-1}.

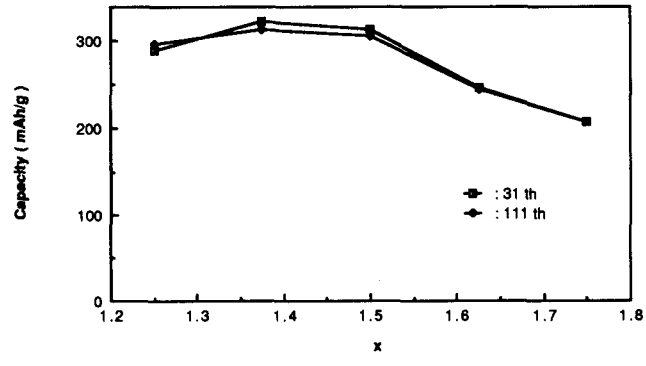

Fig. 10. Comparison of hydrogen storage capacities at cycles 31 and 111 for $Zr_{0.5}Ti_{0.5}V_{0.75}Ni_x$ alloys (charged at 200 mA g^{-1} for 2 h, held for 10 min, discharged at 50 mA to 0.55 V vs. Hg/HgO at 20 °C).

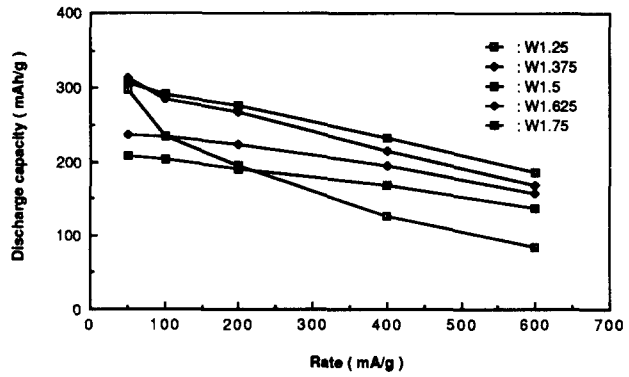

Fig. 11. Comparison of discharge capacity vs. discharge rate curves for $Zr_{0.5}Ti_{0.5}V_{0.75}Ni_x$ alloys (charged at 200 mA g^{-1} for 2 h, held for 10 min, discharged to 0.55 V vs. Hg/HgO at 20 °C).

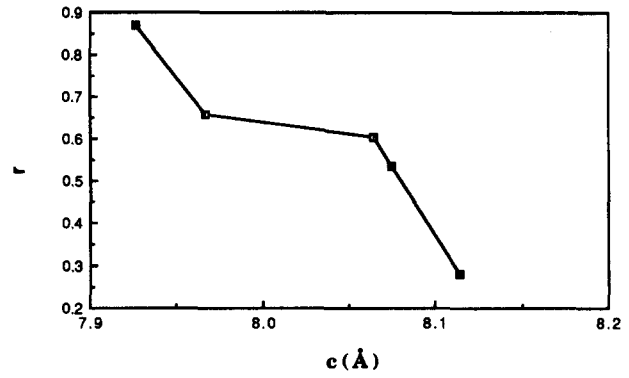

Fig. 12. Effect of axial lattice parameter c on r (see text) of $Zr_{0.5}Ti_{0.5}V_{0.75}Ni_x$ alloys.

at 600 mA g^{-1} to the hydrogen capacity at 50 mA g^{-1} for the W_x alloys. It is thus a parameter reflecting the hydrogen capacity and discharge rate property, which is influenced by the alloy microstructure.

The dissolution behaviour of W_x with dendrite-free structure in electrolyte has been investigated by ICPS. The ICPS analysis shows that V forms soluble oxide which easily dissolves in alkaline solution. For the $W_{1.5}$ alloy, after 94 electrochemical C–D cycles the ionic concentrations of Zr, Ti, V and Ni in electrolyte solution are 3.41, 0.027, 9.51 and 0.073 ppm respectively. This dissolution increases the electrode surface area and microporosity and thereby increases the charge acceptance. The primary role of Zr, Ti and V is hydrogen storage, so the dissolution of V and Zr causes the capacity of the alloy to decrease.

In the alloys Ni plays a crucial role. In $W_{1.25}$ the M–H bonding strength of Zr, Ti and V is too strong and cannot ensure sufficient charge and discharge reaction rates. An increase in Ni content can control the alloy–H bonding strength to a suitable level and benefit electrochemical applications. Ni is a catalyst for the electrochemical reaction $M + H_2O + e^- \rightarrow MH + OH^-$. During C–D cycling, the alloy surface disproportionates into oxides of Zr, Ti and V and metallic Ni which is decentralized in the oxides. The activation of the alloy

Table 3
Maximum discharge capacity C_{max} and cycle life data of W_x alloy electrodes at various discharge rates (charged at 200 mA g^{-1} for 2 h, held for 10 min, discharged to 0.55 V vs. Hg/HgO at 20 °C)

Alloy	C_{max} (mA h g^{-1})			
	200 mA g^{-1}	400 mA g^{-1}	600 mA g^{-1}	C_{300}/C_{max} (%)
$W_{1.25}$	194	126	83	99.9
$W_{1.375}$	267	214	168	80.5
$W_{1.5}$	275	227	190	88.7
$W_{1.625}$	224	223	160	98.8
$W_{1.75}$	193	170	138	99.8

becomes easier with increased Ni content because of the higher concentration of metallic Ni in the oxide films on the alloy surface. An increase in Ni content can improve the electrical conductivity and catalytic activity of oxide films and the corrosion resistance to oxidation.

4. Conclusions

It should be possible to improve the electrocatalytic activity of AB_2 cathodic hydrogen storage alloys by forming a dendrite-free structure. AB_2 alloys with dendrite-free structure exhibit excellent homogeneity and can be easily produced by increasing the Ni content. It was found that the activation and kinetics of W_x ($Zr_{0.5}Ti_{0.5}V_{0.75}Ni_x$, $x=1.375$–1.75) alloys with dendrite-free structure were better than those of the corresponding AB_2 alloy $Zr_{0.5}Ti_{0.5}V_{0.75}Ni_{1.25}$ with dendritic structure. Furthermore, the $W_{1.375}$ and $W_{1.5}$ alloys show higher discharge capacity, while $W_{1.625}$ and $W_{1.75}$ exhibit better durability. Thermal treatment is effective to improve the homogeneity of both dendritic and dendrite-free alloys.

Acknowledgments

The authors wish to express their thanks to Dr. X.-L. Wang for the structure analysis and to Ms. F.-J. Liu for the alloy preparation.

References

[1] H. Sawa, S. Wakao and J. Furukawa, *Denki Kagaku, 58*(9) (1990) 862.
[2] D.-Y. Tan, G. Sandrock and S. Suda, Activation of $Zr_{0.5}Ti_{0.5}V_{0.75}Ni_{1.25}$ electrodes by hot alkaline solutions, *J. Alloys Comp.*, in press.
[3] H. Miyamura, T. Sakai, N. Kuliyama, K. Oguro, A. Kato and H. Ishikawa, *Electrochem. Soc. Proc., 92-5* (1992) 179–198.
[4] S.R. Ovshinsky, M.A. Fetcenko and J. Ross, *Science, 260* (1993) 176–181.